A Thioether-Ligated Cupric Superoxide Model with Hydrogen Atom Abstraction Reactivity

Mayukh Bhadra,[‡] Wesley J. Transue,[ψ] Hyeongtaek Lim,[ψ] Ryan E. Cowley,[ψ] Jung Yoon C. Lee,[‡] Maxime A. Siegler,[‡] Patrick Josephs,[λ] Gerald Henkel,[λ] Markus Lerch,[ε] Siegfried Schindler,[ε] Adam Neuba,[λ] Keith O. Hodgson,[ψ,§] Britt Hedman,[§] Edward I. Solomon[ψ,§,]* and Kenneth D. Karlin[‡,]*

[‡]Department of Chemistry, The Johns Hopkins University, Baltimore, Maryland 21218, United States
[ψ]Department of Chemistry, Stanford University, Stanford, California 94305, United States
[λ]Department of Chemistry, University of Paderborn, Paderborn D-33098, Germany
[ε]Institute of Inorganic and Analytical Chemistry, Justus-Liebig University of Gießen, Giessen D-35392, Germany
[§]Stanford Synchrotron Radiation Lightsource, SLAC National Accelerator Laboratory, Stanford University, Menlo Park, California 94025, United States

Contents :

1. Materials, Methods and Instrumentation

All starting materials used were commercially available analytical grade from Sigma-Aldrich and TCI chemicals. Inhibitor-free 2-methyltetrahydrofuran (2-MeTHF) was purchased from Sigma-Aldrich, distilled under argon from sodium/benzophenone, and sparged with argon prior to use. Acetonitrile was stored under N_2 and purified via passage through 2 cm × 60 cm columns of activated alumina (Innovative Technologies Inc.). Pentane was freshly distilled from calcium hydride under an inert atmosphere and degassed prior to use. Acetone was distilled over regular Drierite (>99.5% $CaSO_4$) under Ar and deoxygenated with Ar before use. Freshly distilled and Ar-sparged Acetonitrile and THF were stored in the glovebox over 3 Å activated molecular sieves and 2-MeTHF over 4 Å activated molecular sieves for at least 2 days prior to use. $[Cu^I(CH_3CN)_4]B(C_6F_5)_4$,[1] TMG_3tren,[2,3-5] $[(^{TMG3tren}N_4)Cu^I]B(C_6F_5)_4$ $([2]B(C_6F_5)_4)$,[6] and TMG-N_3S[7], and TEMPO–H/D[8-9] were synthesized according to literature protocols, and their purities were verified by elemental analysis and/or ^1H NMR. For cyclic voltammetry, tetra-*n*-butylammonium hexafluorophosphate (TBAPF_6) was recrystallized from ethanol before use. Synthesis and manipulations of copper salts were performed according to standard Schlenk techniques or in a VAC (Vacuum Atmospheres Company) glovebox (with O_2 and H_2O levels below 1 ppm).

Bench-top low-temperature UV–visible experiments were carried out on a Cary Bio-50 spectrophotometer equipped with a liquid nitrogen chilled Unisoku USP-203-A cryostat using a 1 cm modified Schlenk cuvette. NMR spectroscopy was performed on Bruker 300 and 400 MHz instruments with spectra calibrated to either internal tetramethylsilane (TMS) standard or to a residual protio solvent.[10] EPR measurements were performed on an X-Band Bruker EMX CW EPR controlled with a Bruker ER 041 XG microwave bridge operating at X-band (~9 GHz) in 5

mm quartz EPR tubes cooled to 77 K in a finger Dewar (Wilmad). Single crystal X-ray Diffraction was performed on suitable crystals, which were mounted either on the tip of a glass fiber or on a loop with a tiny amount of Paratone-N oil and transferred to a N_2 cold stream (110(2) K).

$[(^{TMG}N_3S)Cu^I]B(C_6F_5)_4$ ($[1]B(C_6F_5)_4$) was synthesized as follows: In a 250 ml Schlenk flask in the glove box, 157.9 mg (~0.41 mmol) of $^{TMG}N_3S$ ligand (mol wt = 387.63 grams/mol) were dissolved in 7 mL of 2-MeTHF. 0.9 equivalents of $[Cu^I(CH_3CN)_4]B(C_6F_5)_4$ (336.2 mg, mol wt = 906.79 grams/mol) was added to the solution slowly, yielding a dark yellow solution which was allowed to stir for 5 min after which approximately 100 mL of degassed pentane were added to the copper(I) solution. The bilayered mixture was allowed to sit undisturbed overnight and the solvents were allowed to mix. The supernatant was then decanted and the pale-yellow oil was removed from the glove box and dried under vacuum for 10 min affording a semi-crystalline bright yellow powder which was further dissolved again in 2-MeTHF and recrystallization from pentane resulted in bright yellow crystals of diffraction quality (used for X-Ray crystallography) (87% yield). Elemental analysis: Calcd for $C_{42}H_{41}BCuF_{20}N_7S$: **C**, 44.63; **H**, 3.66; **N**, 8.68. Found: **C**, 44.60; **H**, 3.64; **N**, 7.95.

2. Single Crystal X-Ray Crystallography of $[1]B(C_6F_5)_4$

All reflection intensities were measured at 110(2) K using a SuperNova diffractometer (equipped with Atlas detector) with Cu $K\alpha$ radiation (λ = 1.54178 Å) under the program CrysAlisPro (Version 1.171.36.32 Agilent Technologies, 2013). The same program was used to refine the cell dimensions and for data reduction. The structure was solved with the program SHELXS-2014/7 (Sheldrick, 2015) and was refined on F^2 with SHELXL-2014/7 (Sheldrick, 2015). Analytical numeric absorption correction using a multifaceted crystal model was applied using CrysAlisPro. The temperature of the data collection was controlled using the system Cryojet (manufactured by Oxford Instruments). The H atoms were placed at

calculated positions using the instructions AFIX 23 or AFIX 137 with isotropic displacement parameters

having values 1.2 or 1.5 Ueq of the attached C atoms. The structure is ordered.

Table S1. Experimental details

	[**1**]B(C$_6$F$_5$)$_4$
Crystal data	
Chemical formula	C$_{24}$BF$_{20}$·C$_{18}$H$_{41}$CuN$_7$S
M_r	1130.23
Crystal system, space group	Triclinic, P-1
Temperature (K)	110
a, b, c (Å)	13.7877 (3), 13.9488 (4), 25.8489 (5)
α, β, γ (°)	79.8825 (19), 81.9382 (18), 74.458 (2)
V (Å^3)	4692.2 (2)
Z	4
Radiation type	Cu $K\alpha$
μ (mm^{-1})	2.17
Crystal size (mm)	0.50 × 0.12 × 0.05
Data collection	
Diffractometer	SuperNova, Dual, Cu at zero, Atlas
Absorption correction	Analytical *CrysAlis PRO*, Agilent Technologies, Version 1.171.36.32 (release 02-08-2013 CrysAlis171 .NET) (compiled Aug 2 2013,16:46:58) Analytical numeric absorption correction using a multifaceted crystal model based on expressions derived by R.C. Clark & J.S. Reid. (Clark, R. C. & Reid, J. S. (1995). Acta Cryst. A51, 887-897)
T_{min}, T_{max}	0.579, 0.902
No. of measured, independent and observed [$I > 2\sigma(I)$] reflections	59936, 18322, 16042
R_{int}	0.040
(sin θ/λ)$_{max}$ (Å^{-1})	0.616
Refinement	
$R[F^2 > 2\sigma(F^2)]$, $wR(F^2)$, S	0.038, 0.105, 1.03
No. of reflections	18322

No. of parameters	1315
H-atom treatment	H-atom parameters constrained
$\Delta\rho_{max}$, $\Delta\rho_{min}$ (e Å^{-3})	0.55, -0.56

Computer programs: *CrysAlis PRO*, Agilent Technologies, Version 1.171.36.32 (release 02-08-2013 CrysAlis171 .NET) (compiled Aug 2 2013, 16:46:58), *SHELXS2014*/7 (Sheldrick, 2015), *SHELXL2014*/7 (Sheldrick, 2015), *SHELXTL* v6.10 (Sheldrick, 2008)

Reference: Sheldrick, G. M. (2015). Acta Cryst. C71, 3-8.

3.   Oxygenation of [1]B(C$_6$F$_5$)$_4$ to form [1·O$_2$]B(C$_6$F$_5$)$_4$

In a general procedure, a stock solution of 2.0 mM [**1**]B(C$_6$F$_5$)$_4$ was made by dissolving the solid complex in 2-MeTHF in a scintillation vial in the glovebox. This was further diluted to 0.4 mM and 2.5 ml of this solution was transferred in a Schlenk cuvette via syringe, capped with septum, secured with parafilm, and taken out of the glovebox. The cuvette was allowed to cool to −135 °C in the cryostat of the UV–Vis spectrophotometer for 15 min and then dioxygen was gently bubbled through a metallic needle. Dioxygen was bubbled over 5–6 minutes in intervals of 30 s, giving full conversion to [**1**·O$_2$]B(C$_6$F$_5$)$_4$. At this point, the spectrum was recorded (Figure **S1**). The solution containing [**1**·O$_2$]$^+$ was subjected to vacuum–argon cycles and Ar-bubbling to remove excess O$_2$ and subsequently warmed up to room temperature following which the cuvette was cooled back to −135 °C and the spectrum was recorded while cooling. Figure **S2** depicts the reversible regeneration of [**1**·O$_2$]$^+$. The blue spectrum (Figure **S1**) corresponds to the warmed-up RT product which reversibly binds the released O$_2$ from the cuvette-headspace over a period of ~10 minutes upon gradual cooling of the solution back to −135 °C. Comparison of the 442 nm absorbance (green spectrum of Figures **S1** and **S2**) indicates ~95% regeneration of [**1**·O$_2$]$^+$.
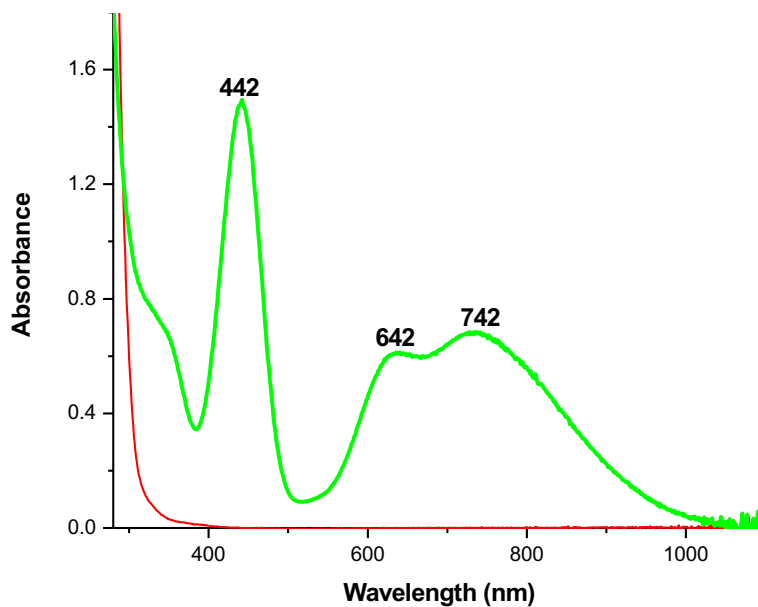
Figure S1. Generation of [**1**·O$_2$]B(C$_6$F$_5$)$_4$ features (green spectrum) from the Cu^I precursor (red spectrum), 0.4 mM solution of [**1**]B(C$_6$F$_5$)$_4$, upon dioxygen addition at –135 °C.
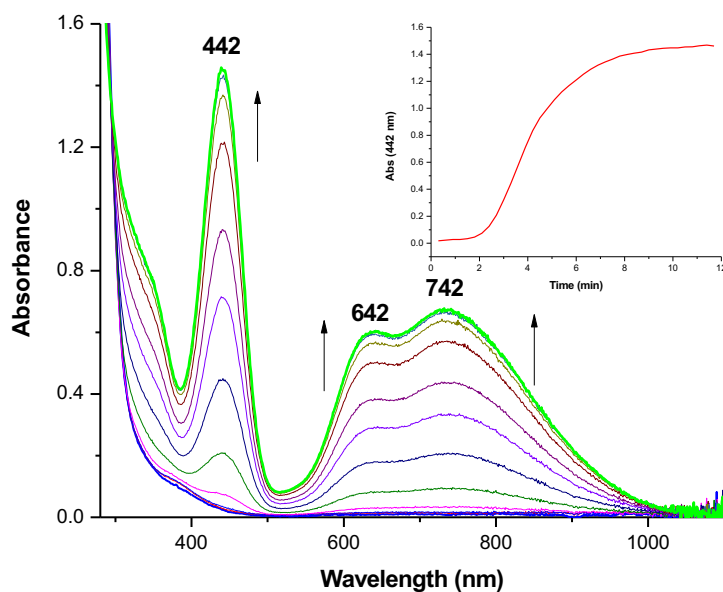

Figure S2. Reversible regeneration of [**1**·O$_2$]B(C$_6$F$_5$)$_4$ features (green spectrum) from the warmed up solution at RT (blue spectrum), upon re-cooling back to –135 °C; (inset) time trace of the growth of the 442 nm band of [**1**·O$_2$]B(C$_6$F$_5$)$_4$, as recorded while gradual cooling of the experimental setup to –135 °C.

4. Thermodynamics of Dioxygen Binding

In a cuvette, a 2.5 ml 2-MeTHF solution of [**1**]B(C_6F_5)$_4$ was taken and excess dioxygen gas was bubbled through a metallic needle in the pre-chilled cuvette in the cryostat. After the full formation of [**1**·O_2]$^+$, the headspace and the solution were purged with alternating vacuum and argon cycles. Starting from the lowest temperature, the cuvette was slowly warmed up at increments of 5–10 °C, the headspace O_2 was carefully equilibrated to 1 atm pressure via a mineral oil bubbler and the solution was kept at each temperature for ~15 min, and then the spectra are recorded. Figure **3a** in the main manuscript summarizes the spectral change corresponding to the decay of [**1**·O_2]$^+$ over a range of –145 to –85 °C.

The temperature-dependent absorbance at 740 nm is plotted in Figure **3b** (orange plot) in the main manuscript. Slowly warming a solution of [**1**·O_2]$^+$ saturated with O_2 (–145 to –85 °C) allowed quantification of [**1**·O_2]$^+$ at several temperatures. At –125 °C, ca. 50% remained and no [**1**·O_2]$^+$ was observed above –90 °C. Analogous measurements on [**2**·O_2]B(C_6F_5)$_4$ (–85 to +15 °C) generated from [**2**]B(C_6F_5)$_4$ were carried out and the spectral changes are shown in Figure **S3** below, revealing the inflection point of the curve to be ca. –40 °C (Figure **3b** (blue plot) in the main text).
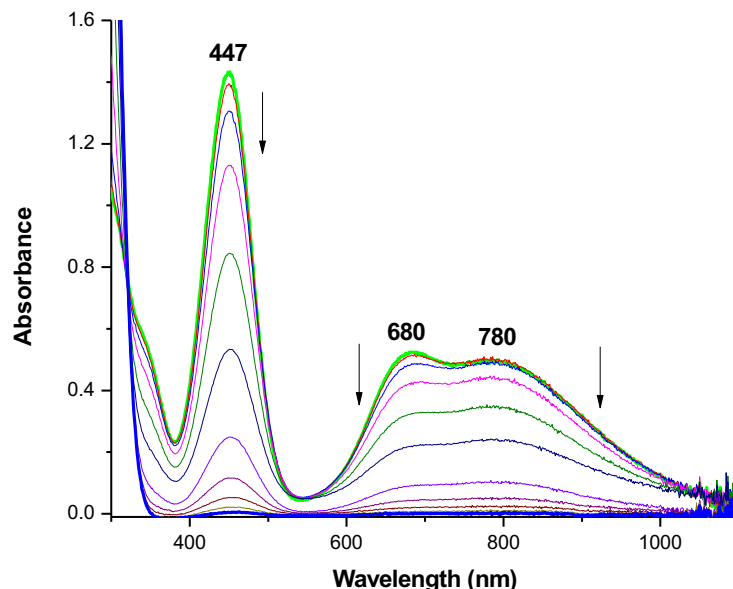
Figure S3. Decay of the $[2 \cdot O_2]^+$ features upon incremental warming of the superoxide solution from –85 °C (green spectrum) to +15 °C (blue spectrum). The temperature-dependent absorbance at 740 nm is plotted in Figure **3b** (blue plot) in the main text.

The relative thermodynamics of dioxygen binding by $[1]B(C_6F_5)_4$ and $[2]B(C_6F_5)_4$ were quantified by fitting the variable temperature UV–Vis data at 740 nm for superoxide formation. This wavelength was selected because it is positioned centrally within the ligand field transitions of both $[1 \cdot O_2]^+$ and $[2 \cdot O_2]^+$. Additionally, it avoids the ~680 nm region, as the 680 nm band of $[2 \cdot O_2]^+$ appears to narrow slightly at the lowest temperatures measured. Such a lineshape change would skew single-wavelength fits. Similar fits to those at 740 nm are obtained at 447 and 780 nm wavelengths.

The relation between equilibrium constant $K_{eq} = \frac{[CuO_2]}{[Cu][O_2]}$ and free energy is $\Delta G = \Delta H - T\Delta S = -RT \ln K_{eq}$, where $[CuO_2]$ is the concentration of the superoxide complex $[1 \cdot O_2]^+$ or $[2 \cdot O_2]^+$, $[Cu]$ the concentration of the cuprous complex $[1]^+$ or $[2]^+$, $[O_2]$ the concentration of dissolved oxygen, ΔH the enthalpy change, ΔS the entropy change, R the gas constant, and T the temperature.

Application of balance allows conversion into $[CuO_2] = \frac{[Cu]_{initial}}{1+\exp\left(\frac{\Delta H - T\Delta S}{RT}\right)/[O_2]}$, where $[Cu]_{initial}$ is the initial concentration of $[\mathbf{1}]^+$ or $[\mathbf{2}]^+$ before O_2 introduction. Accurate O_2 solubility data for 2-MeTHF are lacking, so we instead assume it follows Henry's law, giving $[O_2] = \mathcal{H}_0 \exp\left[-\frac{\Delta H_{sol}}{R}\left(\frac{1}{T} - \frac{1}{T_0}\right)\right]$ for a reference solubility $\mathcal{H}_0$ at some reference temperature T_0 and enthalpy of dissolution ΔH_{sol}. Combination of everything with Beer's law gives the superoxide absorption to be $A_{CuO2} = \frac{\alpha}{1+\exp{(\beta + \gamma/T)}}$, where $\alpha = \epsilon l[CuO_2]$ for extinction coefficient ε (740 nm) and cuvette path length l, $\beta = -\ln\mathcal{H}_0 - \frac{\Delta S}{R} - \frac{\Delta H_{sol}}{RT_0}$, and $\gamma = -\frac{\Delta H_{sol}}{R}$. By comparing fitted values of composite variables "β" and "γ", we obtain relative enthalpic ($\Delta\Delta H$ = +3.2 kcal/mol) and entropic ($\Delta\Delta S$ = +3.7 cal/mol K) thermodynamics. The fits are shown in Figure **3b** of the main manuscript.

5. Cyclic Voltammetry (CV) Data

All cyclic voltammograms were collected under an inert argon atmosphere in dry and degassed 17:3 2-MeTHF:Acetone at 25 °C (**Note:** The acetone was necessary to dissolve TBAPF$_6$, which did not dissolve in neat 2-MeTHF). The concentration of the cuprous complexes ($[\mathbf{1}]^+$ or $[\mathbf{2}]^+$) was ~1.0 mM, with TBAPF$_6$ used as the supporting electrolyte (0.1 M concentration). A three-electrode system was used as follows: Ag/AgNO$_3$ (10 mM) in CH$_3$CN as reference electrode; glassy carbon electrode as the working electrode; platinum wire as the counter electrode. All reduction potentials were referenced *vs.* Fc$^{+/0}$ as an external standard under the same conditions. The data obtained are shown in Figure **3c** in the main manuscript.

A similar analysis was performed by dissolving the complexes ([**1**]⁺ or [**2**]⁺) in the "more-coordinating" CH₃CN solvent and the data obtained are shown below in Figure **S4**.
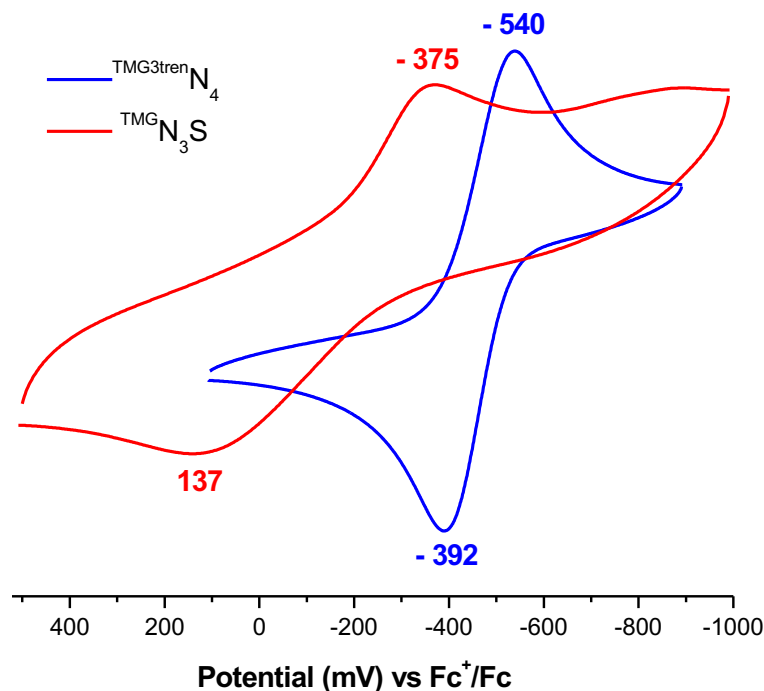
Figure S4. Cyclic voltammograms of the [(L)Cu^I]B(C$_6$F$_5$)$_4$ complexes in MeCN at room temperature under Ar atmosphere. In red is depicted the voltammogram of Cu^{II}/Cu^I couple for [**1**]$^+$/[**1**]$^{2+}$ (L = TMG-N$_3$S) and in blue that for [**2**]$^+$/[**2**]$^{2+}$ (L = TMG$_3$tren). All reduction potentials were referenced *vs.* Fc$^{+/0}$ as an external standard under the same conditions as the [(L)Cu^I]B(C$_6$F$_5$)$_4$ complexes.

6. Resonance Raman Spectroscopy

For resonance Raman (rRaman) measurements, a ~1.0 mM stock solution of [**1**]B(C$_6$F$_5$)$_4$ was prepared in 2-MeTHF in the glovebox. A 500 μL aliquot of this copper(I) solution was added to a 5 mm NMR sample tube, capped with a septum, and chilled in a 2-MeTHF/N$_2$(*l*) bath. Oxygenation of the copper samples was achieved by slowly bubbling an excess of dioxygen through the solution

using a Hamilton gas-tight syringe equipped with a three-way valve and needle outlet. Dioxygen, $^{16}O_2$ (Airgas OX UHP-300) or $^{18}O_2$ (Icon 6393), was added to an evacuated Schlenk flask fitted with a septum for the oxygenation reactions described above. rRaman samples were excited at 413.1 nm using a Coherent I90C-K Kr$^+$ ion laser while the sample was immersed in a liquid nitrogen-cooled (77 K) EPR finger dewar (Wilmad). Power was measured at the sample as 10 mW. Data were recorded while manually rotating the sample to minimize photodecomposition. The spectra were recorded using a Spex 1877 CP triple monochromator with either a 600, 1200, or 2400 groves/mm holographic spectrograph grating, and detected by an Andor Newton CCD cooled to –80 °C. Spectra were calibrated on the energy axis to an external sample of toluene at room temperature. Peak positions were determined from fitting the experimental data with Gaussian transitions using Peakfit Version 4. Figure **3d** in the main text shows the rRaman data obtained for [**1**·O_2]B(C_6F_5)$_4$ with both natural abundance $^{16}O_2$ and $^{18}O_2$.

7. X-Ray Absorption Spectroscopy

The Cu K-edge X-ray absorption spectroscopy (XAS) data were collected at the Stanford Synchrotron Radiation Lightsource (SSRL) on the unfocused 20-pole, 2 T wiggler side-station beam line 7-3 under storage ring parameters of 3 GeV and ~500 mA. A Si(220) double-crystal monochromator was used for energy selection. The M_0 mirror was not employed and the monochromator was detuned by ~50% to remove contributions from higher harmonics. The 2-MeTHF solutions of [**1**]B(C_6F_5)$_4$ and [**1**·O_2]B(C_6F_5)$_4$ were loaded into delrin XAS cells with 38 μm Kapton windows and stored in liquid N_2. During data collection, the samples were maintained at a constant temperature of ~10 K using an Oxford Instruments CF 1208 liquid helium cryostat. A Canberra 30-element Ge solid-state detector and soller slits equipped with a Ni filter were used

to collect Cu Kα fluorescence data. Internal energy calibration was accomplished by simultaneous measurement of the absorption of a Cu foil placed between two ionization chambers situated after the sample. The first inflection point of the foil spectrum was assigned to 8980.3 eV. The extended X-ray absorption fine structure (EXAFS) data are reported to $k = 12.8$ Å^{-1} to avoid interference from the Zn K-edge. Over the course of data collection, [**1**]B(C$_6$F$_5$)$_4$ did not show photodamage, while photoreduction was observed for [**1·O$_2$**]B(C$_6$F$_5$)$_4$. Thus, only the first scans from the fresh sample spots were used for the final average data of [**1·O$_2$**]B(C$_6$F$_5$)$_4$. The data presented here include an average of 24 scans and 19 scans for [**1**]B(C$_6$F$_5$)$_4$ and [**1·O$_2$**]B(C$_6$F$_5$)$_4$, respectively.

Background subtraction and normalization of the data were performed using PySpline.[11] The data were processed by fitting a second-order polynomial to the pre-edge region and subtracting this from the entire spectrum as a background. A three-region spline of orders 2, 3, and 3 was used to model the smoothly decaying post-edge region. The data were normalized by scaling the spline function to an edge jump of 1.0 at 9000 eV. The EXAFS curve-fitting analysis program OPT in EXAFSPAK (George, G. N. Stanford Synchrotron Radiation Laboratory: Stanford, CA, 2000) was used to fit the EXAFS data. The theoretical phase and amplitude functions were generated by FEFF (version 7.0).[12] Starting structural models were obtained from the DFT optimized structures. During the fitting process, the bond distance (R) and the mean-square thermal and static deviation in R (σ^2), which is related to the Debye-Waller factor, were allowed to vary. The threshold energy (E_0), the point at which the photoelectron wave vector k is 0, was also allowed to vary but was constrained as a common value for all components in a given fit. The amplitude reduction factor (S_0^2) was fixed to a value of 1.0 and the coordination number (CN) were systematically varied to achieve the best fit to the EXAFS data and their Fourier transforms.
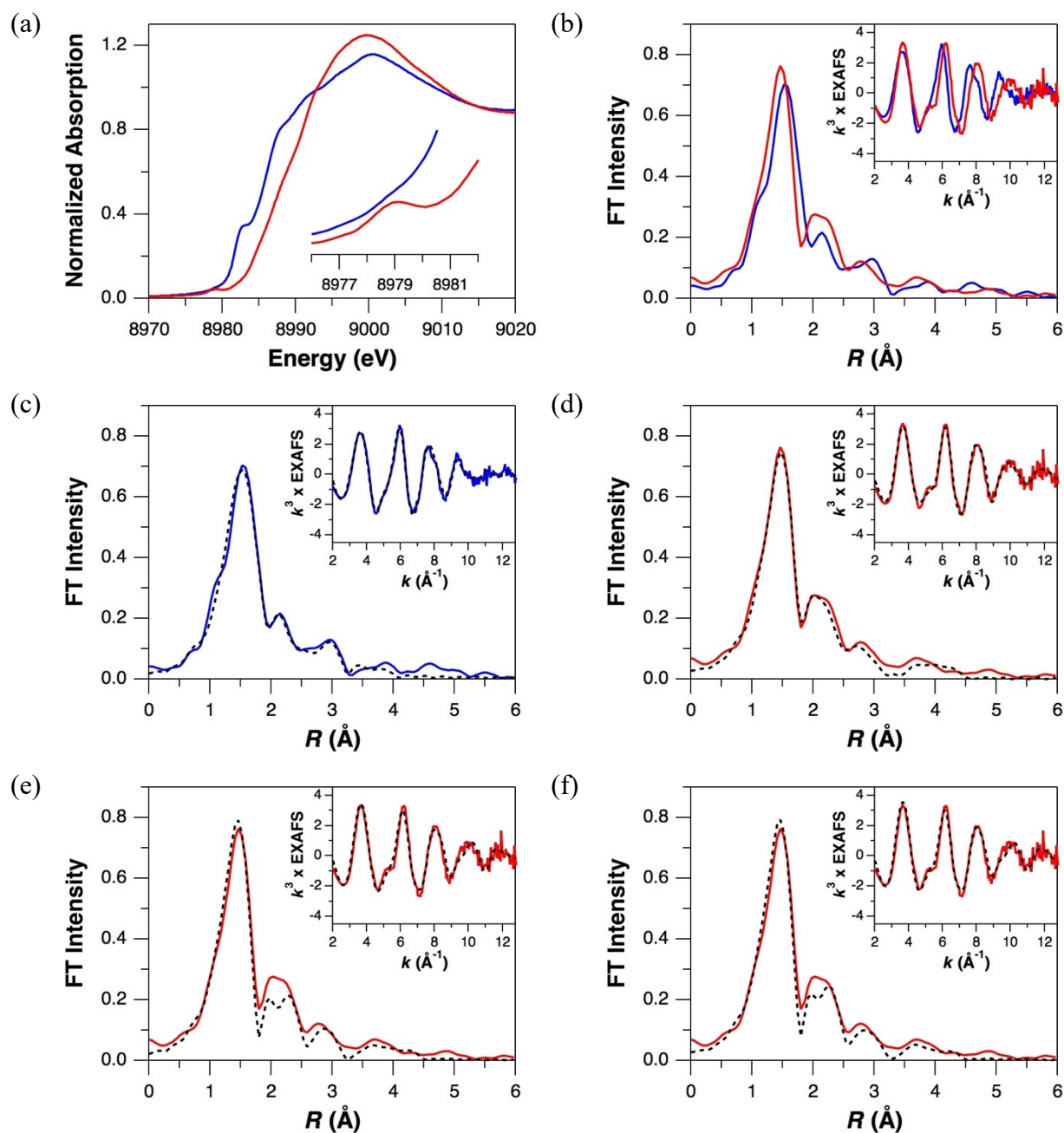
Figure S5. XAS studies on [**1**]B(C₆F₅)₄ (blue) and [**1·O₂**]B(C₆F₅)₄ (red). (a) Cu K-edge XAS spectra of both compounds with an inset showing the expanded pre-edge region. (b) Comparison of Cu K-edge EXAFS data (inset) and non-phase-shift-corrected Fourier transforms. (c, d) Best fits for EXAFS data (data solid, fit dashed). (e, f) Fits for [**1·O₂**]B(C₆F₅)₄ replacing the Cu–S interaction by (e) Cu–C or (f) Cu–O (data solid, fit dashed).

Table S2. Best Fits for the Cu K-edge EXAFS Data

Complex	CN/Path[a]	R (Å)[b]	σ^2 (Å²)[c]	ΔE_0 (eV)	Error F[d]
[**1**]B(C$_6$F$_5$)$_4$	3 Cu-N/O	2.01	824	-13.64	0.17
	1 Cu-S	2.26	651		
	10 Cu-N-C	3.22	822		
	4 Cu-C/N	3.45	839		
	6 Cu-N/C-N/C	4.31	934		
[**1**·O$_2$]B(C$_6$F$_5$)$_4$	4 Cu-O/N	1.98	943	-9.68	0.21
	1 Cu-S	2.55	1171		
	14 Cu-N-C	3.29	504		
	6 Cu-N/C-N/C	4.29	927		
	16 Cu-N/C-N/C	4.66	495		

[a]CN is coordination number. [b]The estimated standard deviations in R are ±0.02 Å. [c]The σ^2 values are multiplied by 10^5. [d]The error F is given by $[\sum k^6(\chi_{exptl} - \chi_{calcd})^2/\sum k^6\chi_{exptl}^2]^{1/2}$. Errors in coordination numbers are ±25% and those in the identity of the scatterer Z are ±1.

Table S3. EXAFS Fitting Results for [1·O$_2$]B(C$_6$F$_5$)$_4$ with Cu-C or Cu-O Contribution

CN/Path[a]	R (Å)[b]	σ^2 (Å^2)[c]	ΔE_0 (eV)	Error F[d]
with Cu-C				
4 Cu-O/N	1.96	948	-12.24	0.25
1 Cu-C	*2.85*	*452*		
14 Cu-N-C	3.29	383		
6 Cu-N/C-N/C	4.24	893		
12 Cu-N/C-N/C	4.63	351		
with Cu-O				
4 Cu-O/N	1.96	947	-12.08	0.24
1 Cu-O	*2.80*	*602*		
14 Cu-N-C	3.30	453		
6 Cu-N/C-N/C	4.25	906		
12 Cu-N/C-N/C	4.63	468		

[a]CN is coordination number. [b]The estimated standard deviations in R are ±0.02 Å. [c]The σ^2 values are multiplied by 10^5. [d]The error F is given by $[\sum k^6(\chi_{exptl} - \chi_{calcd})^2/\sum k^6\chi_{exptl}^2]^{1/2}$. Errors in coordination numbers are ±25% and those in the identity of the scatterer Z are ±1. The Cu-C or Cu-O contribution which replaces the Cu-S contribution in the best fit is indicated with the italic font.

8. Density Functional Theory Computations

Calculations were performed using ORCA 4.2.1[13] at the RIJCOSX-B3LYP-D3(BJ)/Def2-TZVP

level of theory[14-20] with a conductor-like polarizable continuum model[21] to model tetrahydrofuran

solvation. Geometry optimizations were initiated from the crystal structure. The optimized

structures largely agreed with experimental results, showing an increase in copper–sulfur distance

upon O_2 binding (calculated 2.32 Å to 2.50 Å; experiment 2.27 Å to 2.55 Å). Comparison of

vibrational levels with experiment was complicated by mixing of modes with the ligand, but a

weighted average gave 378 cm^{-1} (Cu–O) and 1173 cm^{-1} (O–O).

8.1. Optimized Coordinates of [1]$^+$

```
Cu    -0.04516643556445    0.00032479526531    -0.00885512610058
N     -0.05223785932137    -0.01782617142287    -2.27039192911036
C     -1.44175972981732    -0.36919125007648    -2.57312666111229
H     -1.71759512574404    -0.07598841920926    -3.59615796886599
H     -1.53413865345154    -1.45331096032946    -2.50904619457946
C     -2.42350246998953    0.26095303398839     -1.58713067748671
H     -3.43404169365740    -0.06824149083584    -1.84718112607095
H     -2.40560969244515    1.34681560984768     -1.71844681141356
N     -2.08213901902418    -0.10898433006512    -0.21763674566101
C     -3.02239922462542    -0.19495211527417    0.68004449259237
N     -2.82798850098680    -0.93399276597462    1.81400092970899
C     -3.26279311418169    -0.45836584167445    3.11761949088148
H     -3.83938681037761    0.45519288040610     3.01017636908091
H     -3.87457732300594    -1.20570422314509    3.62843945624212
H     -2.39126871806135    -0.24240338453026    3.74399941024732
C     -1.80580495711239    -1.96513784291048    1.85435097471860
H     -0.82893908125248    -1.56397884493047    2.14880187434787
H     -2.10163436753502    -2.72396733922047    2.58109521547119
H     -1.70322225352346    -2.42385490792588    0.87498578710693
N     -4.25379044346487    0.40642204425437     0.56657877299263
C     -5.47800919340446    -0.22545571476135    1.02832194261291
H     -5.89343835099879    0.27844620555042     1.90729892621495
```

H	-6.22593926623366	-0.18841441271607	0.23143560629757
H	-5.28687595028228	-1.26571693820219	1.27711307493158
C	-4.39644447912035	1.75907771608174	0.05935137413341
H	-3.42431767901639	2.23848799115268	-0.00683147776184
H	-4.87202192451293	1.78700461763779	-0.92559825353747
H	-5.01338853170498	2.33711350897725	0.75298591383134
C	0.30876288655164	1.36640937806953	-2.58869992341292
H	0.66796505796465	1.46121093506287	-3.62254147011509
H	-0.58698581970125	1.97890209581045	-2.49940031310166
C	1.36876849778492	1.91345361914001	-1.63247081912706
H	1.57404180068273	2.95510260508116	-1.89756766026532
H	2.30210039652158	1.36481966434874	-1.79210389042714
N	0.91436555819503	1.80097445485727	-0.25020071434891
C	1.31351344049602	2.66684343655218	0.63663459979539
N	0.57766254248374	2.87593129435609	1.77750281756531
C	1.23281534414666	2.95872806032538	3.07642466893744
H	2.30376489610357	3.08448656502855	2.95277645685045
H	0.84095852617790	3.79807703890558	3.65476584901628
H	1.05892003331951	2.03761839823591	3.64399429649317
C	-0.80950988555837	2.46223277519814	1.83046002278683
H	-0.91601495141745	1.40405248013358	2.09951690379009
H	-1.32568266566802	3.06351062998041	2.58093056368088
H	-1.27600310074691	2.61057167184594	0.86122664077159
N	2.44108087487793	3.44167605614597	0.50431454951717
C	2.50869628701587	4.81460828115036	0.97493881311676
H	3.16693263328798	4.91906848377819	1.84381816415649
H	2.89992231399820	5.45066782314878	0.17627104126515
H	1.51512734995333	5.16274038457117	1.24365062454426
C	3.67753013140690	2.89440537736077	-0.02454861042308
H	3.61788212706640	1.81053554975758	-0.06390539025533
H	3.90977160706532	3.27372457814542	-1.02417400140174
H	4.50019139422221	3.16448824465403	0.64306138507072
C	0.92043323896915	-1.00403364412846	-2.73127288127327
H	0.69098872257058	-1.34725932594234	-3.75020816462292
H	1.89823406566090	-0.52693546401876	-2.77867246135361
C	1.00518912019847	-2.23221082172950	-1.82635293054533
H	0.06006290030511	-2.77458254799642	-1.80680190773266
H	1.76610541469768	-2.91947277553722	-2.19480524621220
S	1.33580605955069	-1.85952335072191	-0.06521264817578
C	3.05393553809058	-1.23929997078411	-0.11206523906866
H	3.20361149049926	-0.82182321599591	0.88392447141699
H	3.10201111239157	-0.41409251095453	-0.82057023101982
C	4.09277333687476	-2.30357371967227	-0.42451949528829
H	3.95223784288073	-2.72147913222490	-1.42225467908863
H	5.09197840918264	-1.86346354018284	-0.38674652703178
H	4.04907632031361	-3.11889131171215	0.29874669580428

8.2 Optimized Coordinates of [1·O₂]⁺

```
Cu   0.13435586004532    -0.17339561825732    -0.04636153348699
O    0.20224109574098    -0.22887774765788    1.94536633439382
O    1.40223131722906    -0.25916315008569    2.40723583837849
N    0.08590102857705    -0.18668179114921    -2.24303135388981
C    -1.31955075006380   -0.48401282746371    -2.58979704689674
H    -1.44094531522387   -1.56606207085639    -2.60130166987141
H    -1.55282710204030   -0.10846573091327    -3.59244101453434
C    -2.27432112405880   0.09941504222866     -1.55871458733715
H    -2.22946468311746   1.19231208545163     -1.60166545934042
H    -3.29682370597231   -0.18598736816010    -1.81981219075702
N    -1.89415412444397   -0.40690576573921    -0.24639378718262
C    -2.80378570057920   -0.62394211807643    0.67065188937224
N    -2.58519390278842   -1.55374740083098    1.64084649938911
C    -2.96916256810040   -1.32598649292645    3.02502889358641
H    -2.07562884224263   -1.34663939271903    3.65441613175879
H    -3.66207473247765   -2.09426919355340    3.37796997128741
H    -3.43806266387035   -0.35193051332905    3.12941752830696
C    -1.71673490435906   -2.69376946963370    1.41642546808830
H    -1.61413375463635   -2.86834309667185    0.34923153455775
H    -2.16597834344501   -3.57349117649111    1.88361219450867
H    -0.72477623599889   -2.53979732015059    1.84532443129069
N    -4.00933604407209   0.02165887805609     0.70870194198104
C    -5.23382925424169   -0.63176029455850    1.14368485167284
H    -5.07061595150445   -1.70168011831058    1.23587010636451
H    -6.01430260025072   -0.45918602303386    0.39836899452336
H    -5.58497634931999   -0.24082250874502    2.10322996469711
C    -4.13910065004170   1.42468839374408     0.35680502760371
H    -3.15811594895927   1.88022323156759     0.27560195669525
H    -4.69168250371991   1.94001392859481     1.14645438397475
H    -4.67600768743497   1.56535776177598     -0.58546709498910
C    0.48248017546425    1.18755698353483     -2.61921781237320
H    -0.38111064177802   1.83715250630721     -2.48808947892577
H    0.77598115802380    1.22566079400959     -3.67408042468238
C    1.60669836959366    1.68368835453797     -1.71971973850157
H    2.51075461040644    1.09371144697277     -1.90277474671691
H    1.84922042557563    2.71564698066242     -1.98776586616063
N    1.14561923399675    1.58462220664493     -0.34237894119652
C    1.54259412474483    2.45835762533586     0.55066299208629
N    2.76050297007241    3.07464086768825     0.50272638152456
C    2.96294001652578    4.45526459700286     0.91201608342747
H    2.00287838394012    4.93863411962913     1.06933748613495
H    3.49617121851422    4.98826045985146     0.12096019232042
H    3.55286425637859    4.52669465722564     1.83036095159143
```

C	3.94069886433507	2.37044061168496	0.03298564128352
H	3.74914234511739	1.30151447007174	0.02346600359692
H	4.76651916269547	2.56551533690646	0.72079875576009
H	4.24488484090072	2.68945834048568	-0.96818249866900
N	0.71620593003479	2.81015717695505	1.57257807258090
C	1.20115894693782	3.03152675512541	2.92564884163306
H	2.27401707410404	2.87204800249328	2.96992116667628
H	0.72086993051454	2.31943778050181	3.60120978155630
H	0.97482149843295	4.04463890651608	3.26810643934202
C	-0.72462220972880	2.71263794643258	1.43843602942695
H	-0.98925326240666	2.71789616029764	0.38523123437725
H	-1.18384806393755	3.57293557013547	1.93093648446998
H	-1.11270452895281	1.80018226348780	1.89712489165351
C	1.01234457399234	-1.17545414147890	-2.82366977718518
H	2.00673026319394	-0.73479139250564	-2.85126342127733
H	0.73210287121452	-1.38627571770003	-3.86285529131357
C	1.06545896742557	-2.48143432664520	-2.04725181158702
H	1.77928265916526	-3.16089343539190	-2.51069754901276
H	0.09889907384768	-2.98497474833579	-2.03719776942495
S	1.47874509624294	-2.26166158404241	-0.28765645133434
C	3.19591522859287	-1.64978919536983	-0.33866799850712
H	3.23722062763839	-0.78084669560330	-0.99307969659938
H	3.36423408267787	-1.29812973078602	0.67924687881177
C	4.21633163111759	-2.69920425360896	-0.74628849928143
H	4.18803833571247	-3.55579101968154	-0.07185249553384
H	5.21911838348487	-2.26730869664655	-0.71285319395950
H	4.04172951755915	-3.05535811480632	-1.76260905015685

8.3. Optimized Coordinates of [2]⁺

Cu	-0.02066868611896	-0.00353738230438	-0.21719674693897
N	-0.13934861456512	0.00952207021358	-2.47941092649463
C	0.84379624850358	1.02078067960500	-2.85649290466307
H	0.36509195533370	1.99763932276271	-2.79207069235079
H	1.18369668795239	0.89181293724418	-3.89481542384174
C	2.05956738612561	1.01373831939659	-1.92743035022918
H	2.59695443814516	0.06984238481167	-2.06148835052403
H	2.74291295386593	1.81050392942085	-2.23827178593246
N	1.64331827680089	1.18269423584543	-0.53987251994483
C	2.42778794627239	1.77708690647629	0.30689744789680
N	3.78169097073479	1.95349363157852	0.12539998354209
C	4.47419944433851	3.15589183413655	0.55344854118907
H	3.75252163166573	3.92421913893190	0.81679574151232

H	5.09685009533147	3.52512375837867	-0.26617715946128
H	5.12462032298800	2.97179437563035	1.41557852105311
C	4.62635838401048	0.89276047196243	-0.39113964796595
H	4.06572581502257	-0.03471320653170	-0.45687823844832
H	5.46576799087430	0.73463292074713	0.29286312747340
H	5.03202128561900	1.13064773388654	-1.37927427945655
N	1.91418388984431	2.31343521729842	1.46644459272180
C	2.58028563528556	2.08685707864835	2.74191764019473
H	2.01695241245728	1.36131617118952	3.33981338276969
H	2.65418839187322	3.01571457880125	3.31163671785674
H	3.57885213264877	1.69157990950472	2.58259972510507
C	0.49481909477494	2.58072667648965	1.56780727314647
H	0.11781238838550	2.93225184889906	0.61180327201955
H	0.33495256615331	3.34649493653453	2.32911350274584
H	-0.07692907082839	1.68648809423511	1.84489018119141
C	-1.52990263961043	0.37432220207481	-2.73331015708846
H	-2.13334941594037	-0.53118555784866	-2.67349651643847
H	-1.66542006545831	0.78994612217420	-3.74280654391212
C	-2.05670548989620	1.37723027026846	-1.70488541928769
H	-1.51265361251283	2.31894479189204	-1.82547742868741
H	-3.10685416234539	1.59001018447914	-1.92911970977234
N	-1.89753474071965	0.85458912059276	-0.35242016310504
C	-2.74070455807846	1.18862698680721	0.57703647897832
N	-2.86791912525970	0.41150349240354	1.70710039374425
C	-2.91015349102523	1.03038346669445	3.02544459127472
H	-1.95395869235690	0.88821841099598	3.54228536159037
H	-3.69847915376866	0.58568311660603	3.63663110074922
H	-3.09182496015981	2.09698596429732	2.93760245003152
C	-2.37767738000175	-0.95102774824422	1.69965948498916
H	-2.56497220022312	-1.40457494686310	0.73086380101650
H	-2.89815256952679	-1.51504301632108	2.47572594416580
H	-1.29865145748380	-1.00497935241439	1.89062766736292
N	-3.57634563698908	2.28199252464515	0.51526642002142
C	-4.92781562583146	2.26314545546429	1.04640338994966
H	-5.22069390214681	1.24254072790409	1.27732268204653
H	-5.61556044031062	2.66444455066177	0.29680746918644
H	-5.02333236038136	2.87157018899781	1.95235388079064
C	-3.11073977894397	3.56893978184952	0.03211333557552
H	-2.03334450727627	3.55223126695613	-0.10079395669616
H	-3.34947972822986	4.33823993652272	0.77253685827414
H	-3.57864092351292	3.85065759961126	-0.91608056980558
C	0.21579594670859	-1.36060425577116	-2.83593891753334
H	1.30294802260998	-1.43324965962385	-2.85533333301816
H	-0.14716198364959	-1.62932243255309	-3.83918813810115
C	-0.31866016440920	-2.37346922659614	-1.82161726215918
H	-1.41221273644063	-2.36684077483611	-1.86297207613981

H	0.00165301122458	-3.37500030540004	-2.12584695332909
N	0.15221801657977	-2.04870906755242	-0.48000547220817
C	0.35391320807660	-2.99597928346036	0.38527190646110
N	1.17127310774183	-2.77654158850885	1.47099706499243
C	0.76733811157042	-3.20997147250957	2.80165240210526
H	0.45900639969325	-2.34773645266213	3.40376103605743
H	1.59378659921316	-3.70719246314668	3.31425596187716
H	-0.07139749358356	-3.89633069737145	2.73849716104013
C	2.10264806349867	-1.66847813565355	1.45558930974954
H	2.51333788034841	-1.54561167524769	0.45793964502804
H	2.90868896140009	-1.87798150436208	2.16112997610051
H	1.62551648999683	-0.72198000614111	1.73800535357123
N	-0.17875679502565	-4.26290833119582	0.29282574987475
C	-1.55760976581968	-4.47953423891133	-0.10393237274058
H	-2.08881999610624	-3.53347744524514	-0.14316946427505
H	-2.04981267935930	-5.11462188517722	0.63866400918140
H	-1.63769219707114	-4.96970218688687	-1.07901063476870
C	0.55269280694027	-5.45015785706267	0.69828063979571
H	1.59404366909819	-5.19913843777003	0.88048375216408
H	0.50684721978458	-6.19472051250851	-0.10164065431725
H	0.13385094147460	-5.90099421784626	1.60455984147149

8.4 Optimized Coordinates of [2·O$_2$]$^+$

Cu	0.01067962901335	-0.00852962323727	-0.04193123449543
O	-0.09835855050202	-0.02871037427114	1.94286615744684
O	0.97767745561778	0.06245096679442	2.65198179260781
N	-0.10367247749261	0.01582010038053	-2.23324465368407
C	0.97202496107886	0.91590041338599	-2.68796875054211
H	0.59191794715767	1.93642532076130	-2.66850562996035
H	1.25637280083811	0.68310306478819	-3.72073391554423
C	2.17414612277534	0.82948524813185	-1.75789582386131
H	2.60788203144762	-0.17481028898564	-1.81444775090348
H	2.94052943351158	1.52789948933894	-2.10354036654364
N	1.72056214444567	1.14464515583367	-0.41038287713791
C	2.46761664687562	1.88048822069543	0.37057026776295
N	3.83295903494259	1.95391640987427	0.26354063440314
C	4.57145815073077	3.18783153884494	0.47225244139189
H	3.88282376855185	4.02455562923785	0.54985867928040
H	5.23300253756995	3.35830103158407	-0.38142617502287
H	5.18587443308683	3.14907829826823	1.37708628313019
C	4.63730121814981	0.79429285628031	-0.07339242904558
H	4.03171061390512	-0.10357795814947	-0.02238948243005

H	5.45271608427972	0.70115001622216	0.64908100393837
H	5.07405411534715	0.87196843907248	-1.07356381813712
N	1.89874132060994	2.66111510114593	1.33071560118052
C	2.49873879192613	2.84329237473132	2.64236606158315
H	1.81179817738912	2.47447568585913	3.40738321975344
H	2.70913321347286	3.89813391589183	2.83882608135965
H	3.42207135805837	2.27682442816692	2.71409095048457
C	0.52784629509259	3.11128570780888	1.20808845902986
H	0.24399519854781	3.10848845505129	0.16015708145489
H	0.45469370321609	4.12822037829255	1.60102069200445
H	-0.16522425753510	2.47154534849978	1.75946366971738
C	-1.44446243122649	0.52023046344613	-2.58642473343241
H	-2.13498362650958	-0.32191323999229	-2.58256090856165
H	-1.44038751064045	0.94650008351606	-3.59626721154917
C	-1.92461879919268	1.54227754728088	-1.56656913342880
H	-1.28084903592489	2.42744807425360	-1.61149030162217
H	-2.93322619596346	1.86837010260872	-1.83544782042840
N	-1.88591031237088	0.91486930404204	-0.25502621178175
C	-2.81956299293446	1.15982446600477	0.62382619909998
N	-3.12004626793887	0.23164526483672	1.57936192586419
C	-3.35803773204341	0.60238523737361	2.96430687080709
H	-2.57291669690372	0.17491824875759	3.59454102756161
H	-4.32556113922789	0.23096096609741	3.31281778575113
H	-3.33442870434847	1.68260932419495	3.07434042592293
C	-2.88796057864095	-1.17936505236747	1.34777783726780
H	-2.87293418420817	-1.36691297658539	0.27822327564864
H	-3.70194300821099	-1.74928116072535	1.80320706297986
H	-1.94136022807059	-1.51326467795498	1.77763909689014
N	-3.57685163980970	2.30332931552859	0.64220213676318
C	-4.97536945584352	2.30770902165676	1.03817231478179
H	-5.34365234754087	1.28848454795803	1.11199682510914
H	-5.55962312100936	2.83828254762794	0.28168346519350
H	-5.12654149028965	2.81038868222150	1.99861715682531
C	-3.02301709606427	3.60220166044788	0.30659743144992
H	-1.94605844014877	3.53473588677769	0.20719888823137
H	-3.24972577560008	4.30871931622268	1.10991894654752
H	-3.44105791766214	3.99715178644437	-0.62391252083194
C	0.10239320514359	-1.37290761537383	-2.68530026913023
H	1.17443654494180	-1.55730916005631	-2.73868257832660
H	-0.31365076674015	-1.51498263423279	-3.68947017804808
C	-0.50757362673388	-2.35426263568339	-1.69476584350445
H	-1.59464706694761	-2.22129388658912	-1.67420637915361
H	-0.31747563113720	-3.37461035361740	-2.03884419695101
N	0.09234974044536	-2.09702648038167	-0.39529089662396
C	0.38234969032960	-3.08453221548448	0.40859954195558
N	1.40991052353398	-2.95497475072868	1.29672739607251

C	1.29954565587591	-3.40319753266938	2.67447273269753
H	1.37984702249041	-2.54305962897777	3.34481119151357
H	2.08845666871749	-4.11745680969291	2.92635196235614
H	0.33368409335966	-3.87344377159416	2.83751135064664
C	2.54696106961758	-2.10519928166507	0.99338772755147
H	2.64001983648776	-2.00667026755084	-0.08498911999327
H	3.45011629362384	-2.57786505623754	1.38844079323513
H	2.44407319427446	-1.11341432768634	1.43567128551059
N	-0.25965270044761	-4.29524225893515	0.40614532480163
C	-1.67891862663043	-4.41996894648952	0.13072479706440
H	-2.14069891388723	-3.44051679480991	0.09942511235418
H	-2.15127609953546	-4.99782795752670	0.92988725538816
H	-1.86692608619673	-4.93128445266008	-0.81780695634269
C	0.42698064045089	-5.54311665517901	0.69754873973085
H	1.50023430082717	-5.37901053449124	0.72538279586245
H	0.20279457929784	-6.26744669094578	-0.08994624989664
H	0.10734128505468	-5.96984939071212	1.65324866094951

9. Reactivity and Kinetic Studies

The substrates TEMPO–H (10, 20, 30, 80 mmols) and TEMPO–D (40, 60, 120, 300 mmols) were added to 0.4 mM solutions of $[1 \cdot O_2]B(C_6F_5)_4$ via syringe and allowed to react at –135 °C. Decay of the superoxide band at 742 nm was monitored over time and the pseudo-first-order rate constants were calculated from the fitted exponential slopes. A plot of k_{obs} vs substrate concentration was used to determine the second order rate constant. See Figures **S6-S9** and Table **S4** for details.

The same procedure mentioned above was followed for the reactions of TEMPO–H (20, 30, 40, 50 mmols) with 0.4 mM solutions of $[2 \cdot O_2]B(C_6F_5)_4$. See figures **S10-S11** and Table **S5** for details.
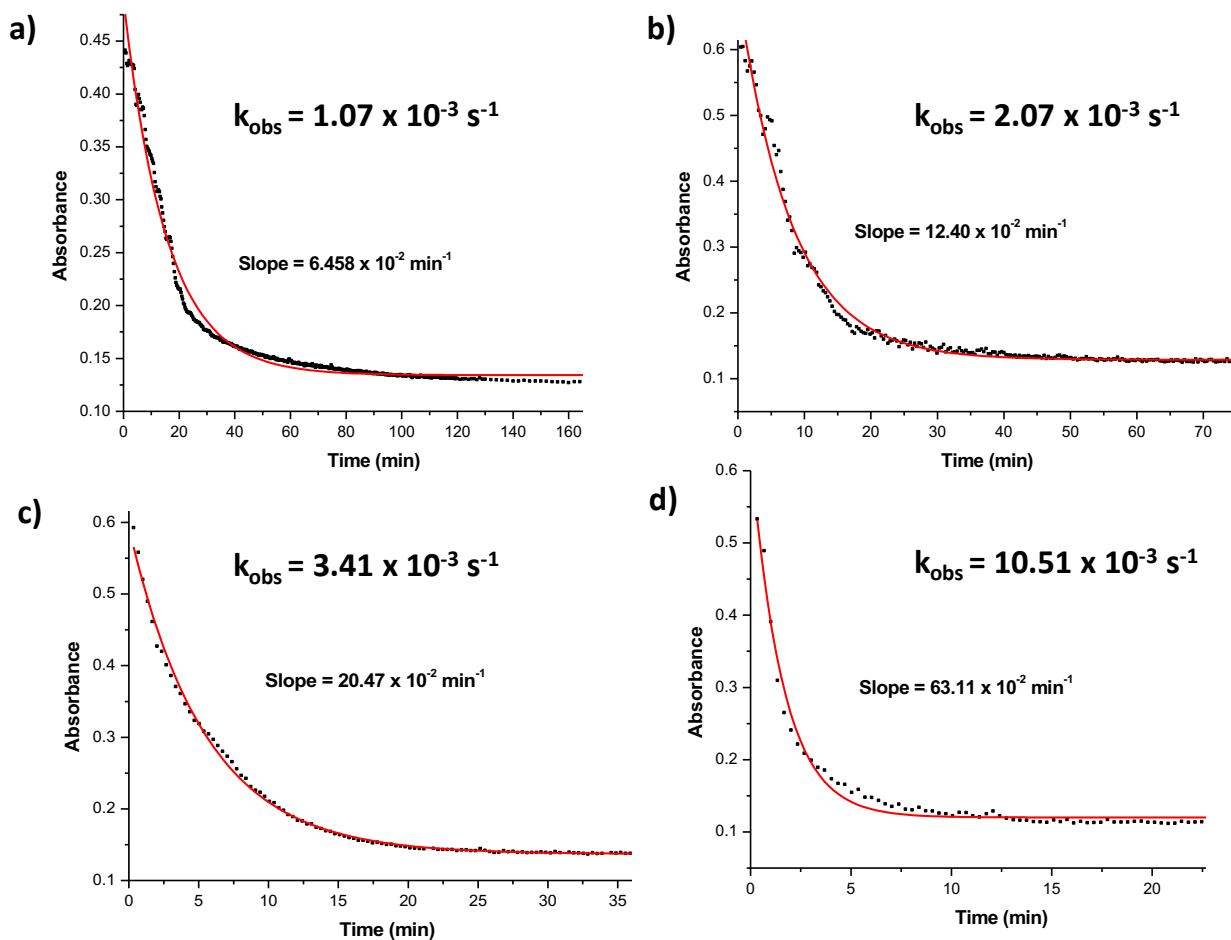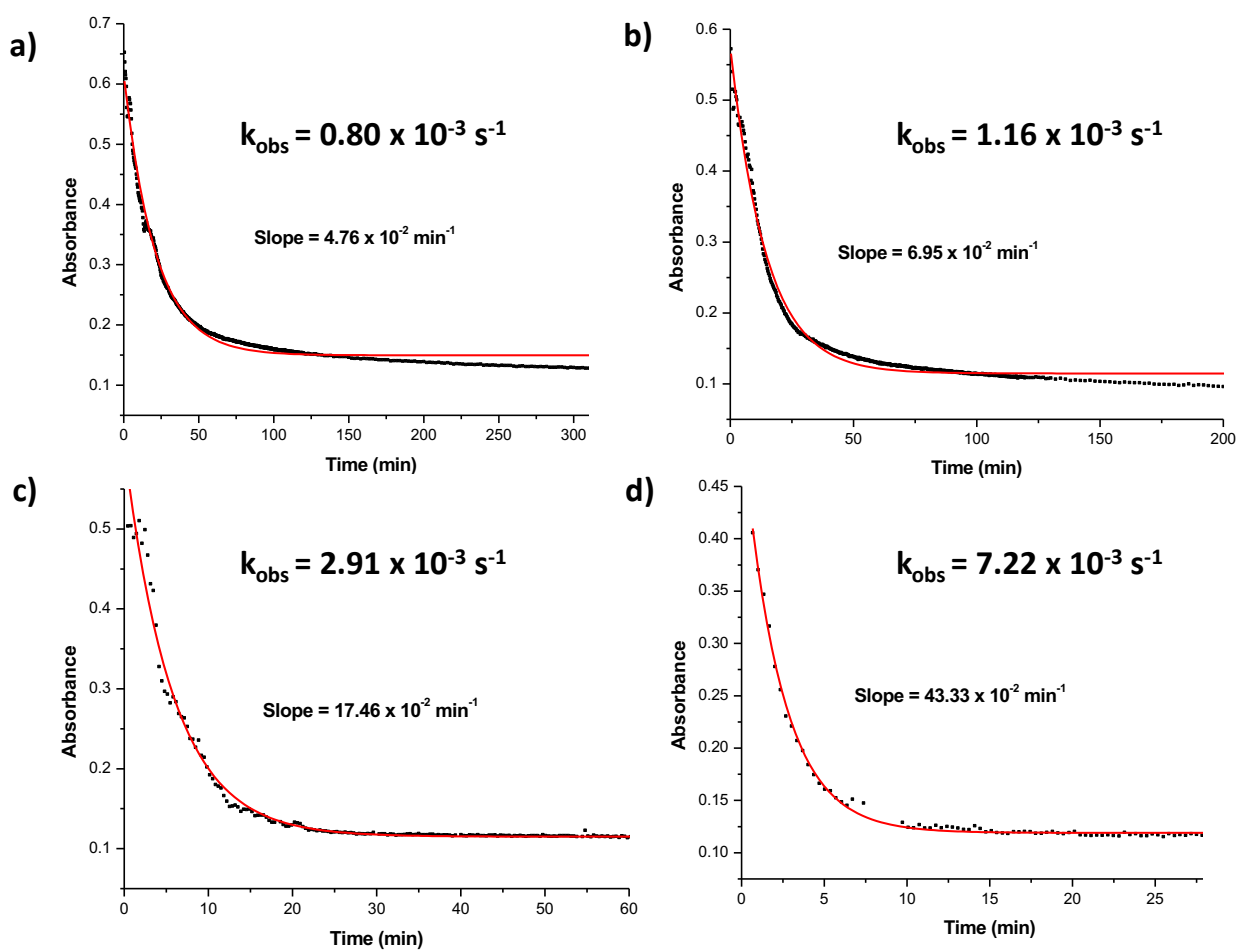
[1·O₂]B(C₆F₅)₄ with TEMPO−H:

Figure S6. Representative exponential plots of absorbance at 742 nm versus time for the reaction of ~0.4 mM [1·O₂]B(C₆F₅)₄ at −135 °C in 2-MeTHF with (**a**) 10, (**b**) 20, (**c**) 30 and (**d**) 80 mmols of TEMPO–H to determine k_{obs} at each concentration. Black dots represent the actual absorbances recorded and the red line is the fitted trace.
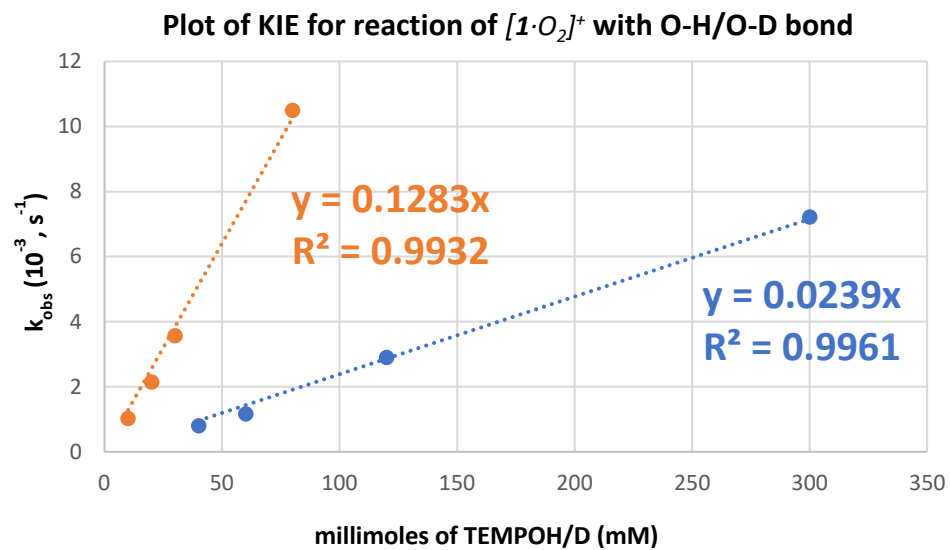
Table S4. Table containing the k_{obs} (s^{-1}) values for the reaction of 0.4 mM [**1**·O$_2$]B(C$_6$F$_5$)$_4$ at −135 °C in 2-MeTHF with 10, 20, 30 and 80 mmols of TEMPO–H.

mol	k_{obs} s^{-1}			Average
	Trial 1	Trial 2	Trial 3	
1.00E-02	1.06E-03	1.07E-03	0.97E-03	1.03E-03
2.00E-02	2.07E-03	2.30E-03	2.09E-03	2.15E-03
3.00E-02	3.10E-03	3.41E-03	4.25E-03	3.57E-03
8.00E-02	0.75E-02	1.05E-02	1.36E-02	1.05E-02

Plot of k_{obs} vs Concentration

y = 0.1283x
R² = 0.9932
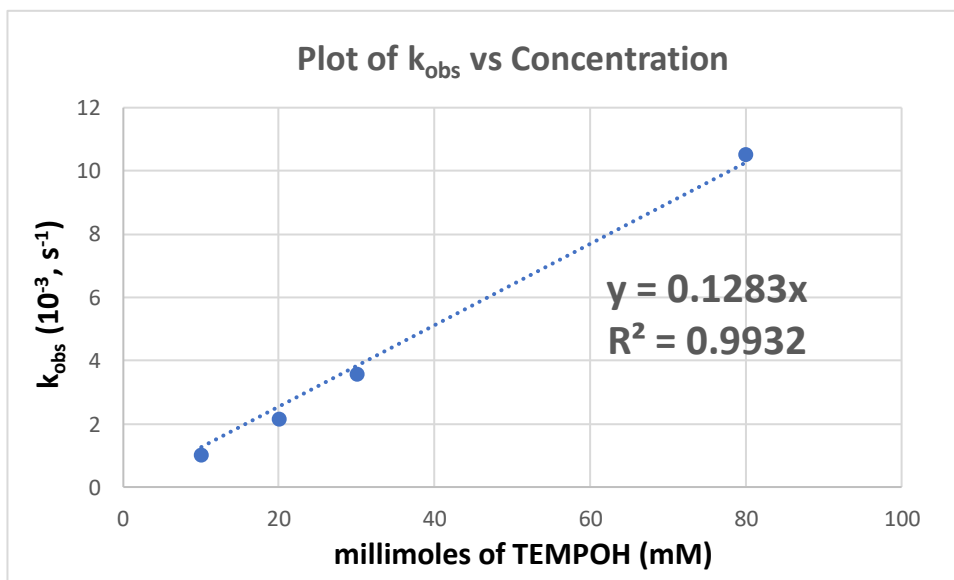
Figure S7. Plot for [**1**·O$_2$]B(C$_6$F$_5$)$_4$ of pseudo-first order rate constants (k_{obs}) against the TEMPO–H concentrations; from the slope of the linear fit, the second-order rate constant is calculated to be 1.28×10^{-1} M^{-1} s^{-1}.

[1·O₂]B(C₆F₅)₄ with TEMPO−D:

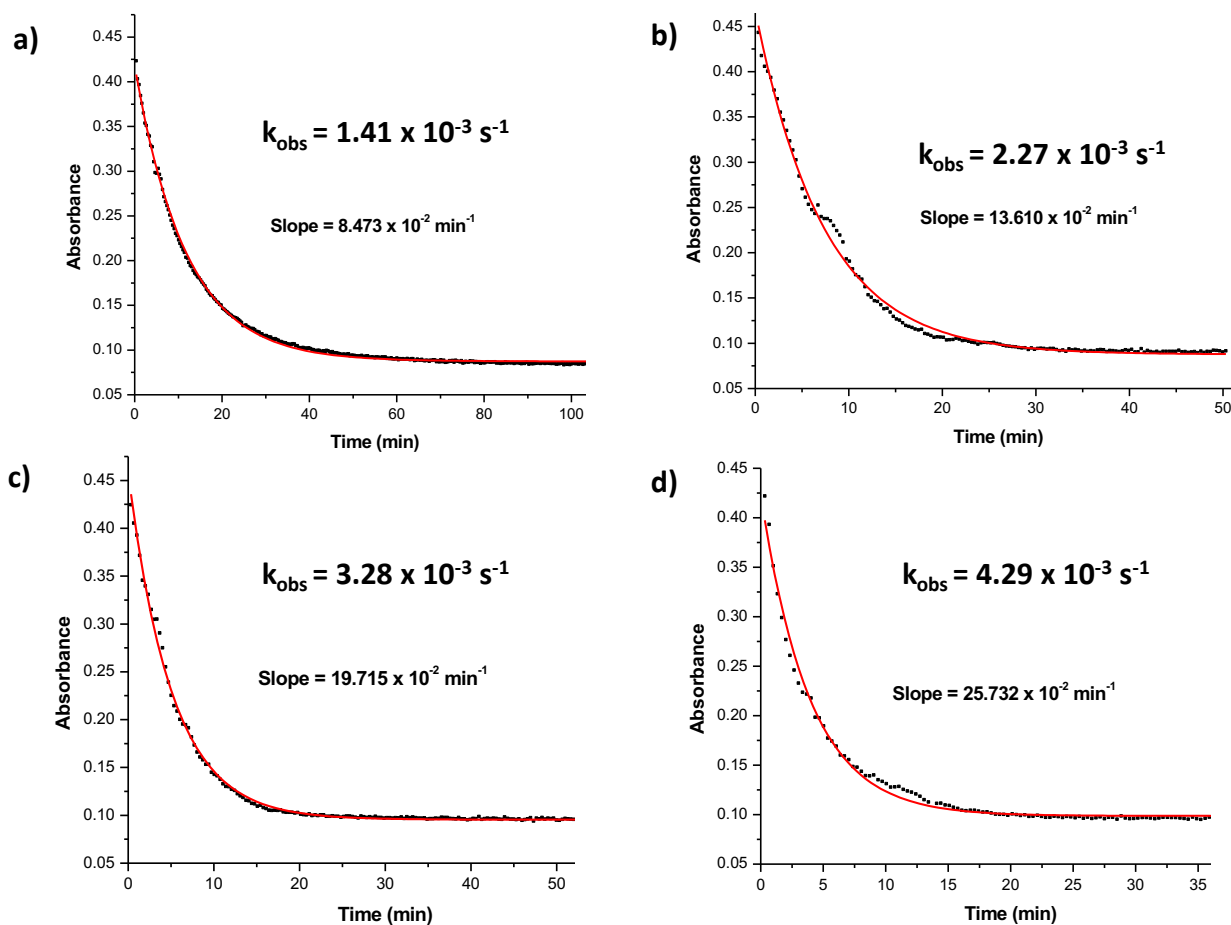**Figure S8.** Representative exponential plots of absorbance at 742 nm versus time for the reaction of ~0.4 mM [**1**·O₂]B(C₆F₅)₄ at –135 °C in 2-MeTHF with (**a**) 40, (**b**) 60, (**c**) 120 and (**d**) 300 mmols of TEMPO–D to determine k_{obs} at each concentration. Black dots represent the actual absorbances recorded and the red line is the fitted trace.

Plot of KIE for reaction of $[1 \cdot O_2]^+$ with O-H/O-D bond

y = 0.1283x
R² = 0.9932

y = 0.0239x
R² = 0.9961

k_{obs} (10^{-3}, s^{-1})

millimoles of TEMPOH/D (mM)

Figure S9. Plots of pseudo first order rate constants (k_{obs}) plotted against various concentrations of TEMPO–H(D) to obtain the second order rate constant, $k_H = 1.28 \times 10^{-1}$ M^{-1}sec^{-1} (orange circle) and $k_D = 0.24 \times 10^{-1}$ M^{-1}sec^{-1} (blue circle) thus yielding a primary KIE of 5.4 in 2-MeTHF at –135 °C, for H-atom abstraction by $[1 \cdot O_2]B(C_6F_5)_4$.

[2·O₂]B(C₆F₅)₄ with TEMPO–H:

Figure S10. Representative exponential plots of absorbance at 780 nm versus time for the reaction of ~0.4 mM [2·O₂]B(C₆F₅)₄ at –135 °C in MeTHF with (**a**) 20, (**b**) 30, (**c**) 40 and (**d**) 50 mmols of TEMPO–H to determine k_{obs} at each concentration. Black dots represent the actual absorbances recorded and the red line is the fitted trace.

Table S5. Table containing the k_{obs} (s^{-1}) values for the reaction of ~0.4 mM [$2 \cdot O_2$]B(C$_6$F$_5$)$_4$ at –135 °C in 2-MeTHF with 20, 30, 40 and 50 mmols of TEMPO–H.

mol	k_{obs} s^{-1}			Average
	Trial 1	Trial 2	Trial 3	
2.00E-02	1.26E-03	1.41E-03	1.55E-03	1.41E-03
3.00E-02	2.27E-03	2.61E-03	2.24E-03	2.37E-03
4.00E-02	3.01E-03	3.49E-03	3.28E-03	3.26E-03
5.00E-02	4.01E-03	4.45E-03	4.29E-03	4.25E-03
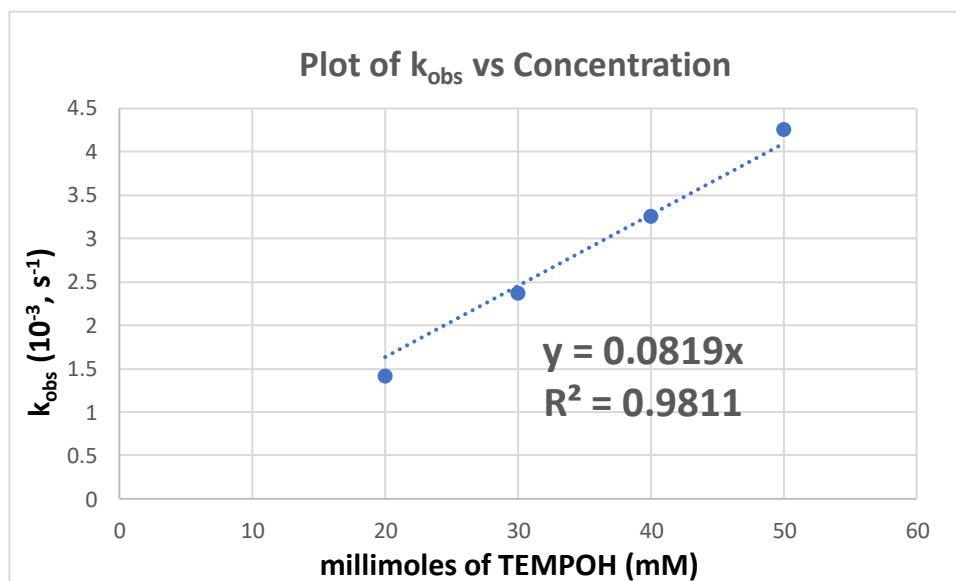
Figure S11. Plot {for [$2 \cdot O_2$]B(C$_6$F$_5$)$_4$} of pseudo first order rate constants (k_{obs}) against the TEMPO–H concentrations; from the slope of the linear fit, the second-order rate constant is calculated to be 0.82×10^{-1} M^{-1} s^{-1}.

Comparison of rates for reaction of $[1 \cdot O_2]^+$ and $[2 \cdot O_2]^+$ with O–H

y = 0.1283x
R² = 0.9932

y = 0.0819x
R² = 0.9811

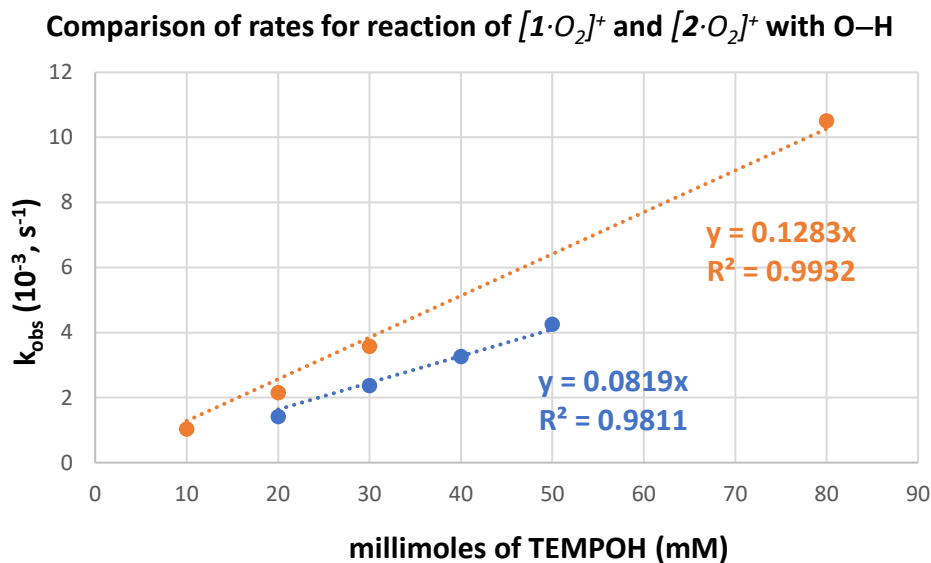x-axis: **millimoles of TEMPOH (mM)**

y-axis: k_{obs} (10^{-3}, s^{-1})

Figure S12. Comparative analysis of rates of hydrogen atom abstraction reactivity with TEMPO–H (2-MeTHF at –135 °C): $k_2 = 1.28 \times 10^{-1}$ M^{-1} s^{-1}, in orange, $[1 \cdot O_2]B(C_6F_5)_4$; 0.82×10^{-1} M^{-1} s^{-1}, in blue, $[2 \cdot O_2]B(C_6F_5)_4$.

10. Product Analyses

A) Quantification of Hydroperoxo Product

The formation (and the yield) of the final cupric hydroperoxo product was further verified by acidification (i.e. liberation of H_2O_2) and subsequent quantification of triodide (I_3^-) formed when treated with a MeCN-saturated solution of I^-. In a typical experiment, 2.5 ml of a 0.80 mM solution of $[1]B(C_6F_5)_4$ in 2-MeTHF was taken in a cuvette in the glovebox, and oxygenated at –135 °C. The superoxide generated was mixed with TEMPO–H and at the end of the HAA reaction, 1 equivalent of $HCl \cdot Et_2O$ (2.0 M, Sigma Aldrich) was added via a syringe (to release H_2O_2) until complete disappearance of the hydroperoxide features is noted via UV-Vis spectroscopy. Then, 150 µL of solution in the cuvette was transferred into a cuvette with saturated NaI solution in MeCN (2.0 mL) at RT. This mixture was allowed to incubate for 6 mins. The UV-Vis spectrum of this solution was then taken showing the formation of triodide (I_3^-) at 362 nm (Figure **S13**). The

yield of H_2O_2 was found to be 94% when compared with standard series of solutions (see Figure S14).[22] Note: (1)Without acidification, $[1 \cdot O_2]B(C_6F_5)_4$ by itself did not show any presence of peroxide formation upon warming and (2) the protonation of the cupric superoxide complex $[1 \cdot O_2]B(C_6F_5)_4$ resulted in 43% yield of H_2O_2, consistent with previous observation of disproportionation of protonated superoxo radical: $2H^+ + 2O_2^{\cdot -} \rightarrow H_2O_2 + O_2$.[22]
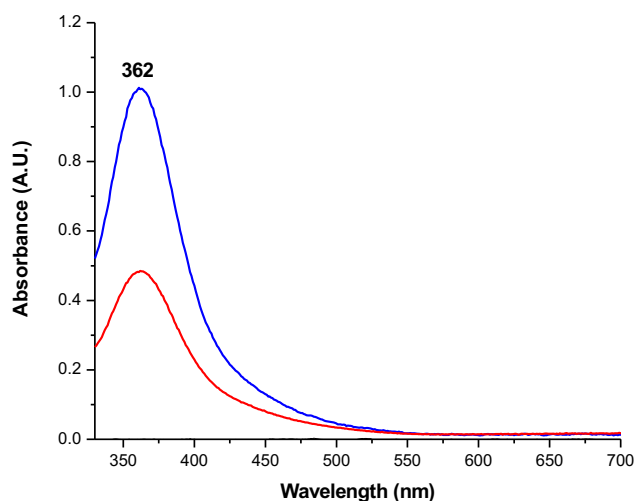
Figure S13. UV-Vis spectra of I_3^- generated ($\lambda_{max} = 362$ nm) from the released H_2O_2 upon addition of 1 equiv of H^+ to the reaction mixture containing $[1 \cdot OOH]B(C_6F_5)_4$ species, in blue and $[1 \cdot O_2]B(C_6F_5)_4$ complex (control), in red.
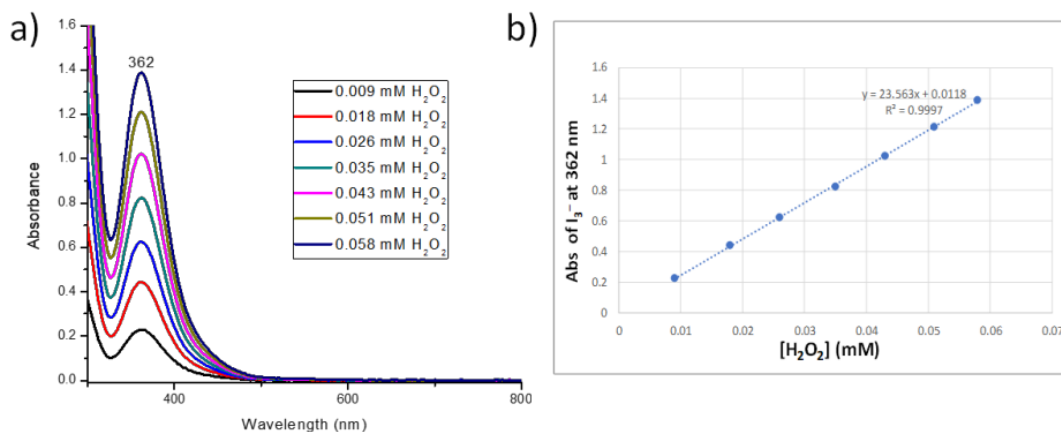
Figure S14. UV-Visible spectrum of triodide (I_3^-) at 362 nm obtained on spectrophotometric titration of I_3^- with H_2O_2 solutions to generate b) the standard linear curve. See *J. Am. Chem. Soc.* **2018**, *140*, 9042-9045 for details.[22]

B) EPR Data

In the glovebox, a 500 ml of 0.8 mM solution of [**1**]B(C_6F_5)$_4$ in 4:1 (v/v) 2-MeTHF:THF was prepared, transferred to an EPR tube and capped with tightfitting septa. The sample tube was placed in a cold bath (4:1(v/v) 2-MeTHF:THF/liq N_2 (−145 °C)) and oxygenated by bubbling dioxygen via a fine-point needle. The oxygenated sample was maintained at −145 °C for ~35 mins and after generation of [**1**·O_2]B(C_6F_5)$_4$, excess TEMPO–H was added to generate TEMPO radical and [**1**·OOH]B(C_6F_5)$_4$. Then, the sample tube was frozen in liquid N_2. Figure **4** in the main manuscript depicts the EPR data obtained. Generations of[**1**·OOH]B(C_6F_5)$_4$ and TEMPO radical are demonstrated by formation of the reverse-axial Cu^{II} features and the sharp radical peak respectively. For quantifying the amount of TEMPO radical formed from this reaction, four different solutions (0.5 mM, 1.0 mM, 1.5 mM, 2.0 mM) of pre-sublimed TEMPO radical in 2-MeTHF were used as standards and the integrated areas corresponding to the Cu^{II}-spins were noted. The amount of TEMPO radical in solution is estimated to be 91%. Similarly, the amount of

[**1**·OOH]B(C$_6$F$_5$)$_4$ species in solution (when compared with the integrated area of an authentic 1.0 mM methanolic solution of Cu^{II}-salt, [**2**·Cl]$^+$, is estimated to be 97%.

Simulation of the EPR data of [**1**·OOH]B(C$_6$F$_5$)$_4$ was challenged by the presence of TEMPO$^\bullet$ and by the peak widths. The g_{zz} and A_{zz}(Cu) values could be clearly seen and were fit to be 2.23 and 370 MHz, respectively. The g_{xx}, g_{yy}, A_{xx}(Cu), and A_{yy}(Cu) values were obscured. The parameters from fitting routines of EasySpin 5.2.3 were g_{xx} 2.02, g_{yy} 2.11, A_{xx}(Cu) 152 MHz, and A_{yy}(Cu) 168 MHz. The simulated spectrum is overlayed with the data in Figure **S15**.
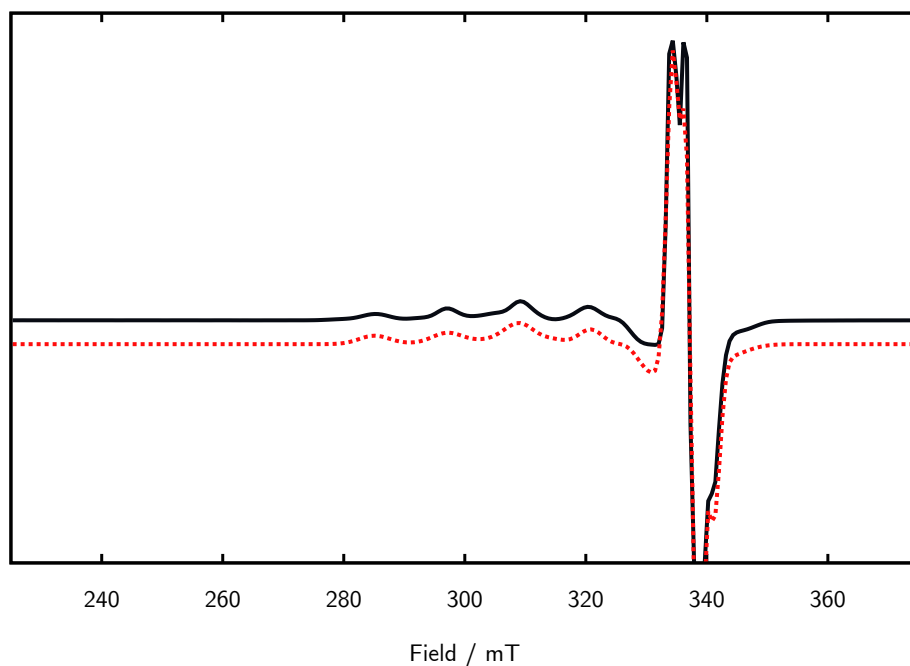

Figure S15. The EPR data could be simulated with EasySpin using best fit copper(II) parameters of g = [2.2303, 2.1143, 2.0185], A = [370.3, 167.9, 152.0] for Nucs = 'Cu', lw = 4.24, gStrain = [0.0278, 0.0244, 0.0407]. The EasySpin parameters for TEMPO$^\bullet$ were g = [2.0082, 2.0052, 2.0022], A = [16.8, 20.4, 95.7] for Nucs = '14N', lw = 1.85, gStrain = [0.0049, 0.0090, 0.0077].

11. References

1.   Liang, H. C.; Kim, E.; Incarvito, C. D.; Rheingold, A. L.; Karlin, K. D. A Bis-Acetonitrile Two-Coordinate Copper(I) Complex: Synthesis and Characterization of Highly Soluble B(C_6F_5)$_4^-$ Salts of [Cu(MeCN)$_2$]$^+$ and [Cu(MeCN)$_4$]$^+$. *Inorganic Chemistry* **2002,** *41*, 2209-2212.

2.   Würtele, C.; Gaoutchenova, E.; Harms, K.; Holthausen, M. C.; Sundermeyer, J.; Schindler, S. Crystallographic characterization of a synthetic 1:1 end-on copper dioxygen adduct complex. *Angewandte Chemie International Edition* **2006,** *45*, 3867-3869.

3.   Wittmann, H.; Raab, V.; Schorm, A.; Plackmeyer, J.; Sundermeyer, J. Complexes of Manganese, Iron, Zinc, and Molybdenum with a Superbasic Tris (guanidine) Derivative of Tris (2-ethylamino) amine (Tren) as a Tripod Ligand. *European Journal of Inorganic Chemistry* **2001,** *2001*, 1937-1948.

4.   Schatz, M.; Raab, V.; Foxon, S. P.; Brehm, G.; Schneider, S.; Reiher, M.; Holthausen, M. C.; Sundermeyer, J.; Schindler, S. Combined Spectroscopic and Theoretical Evidence for a Persistent End-On Copper Superoxo Complex. *Angewandte Chemie International Edition* **2004,** *43*, 4360-4363.

5.   Maiti, D.; Lee, D. H.; Gaoutchenova, K.; Würtele, C.; Holthausen, M. C.; Narducci Sarjeant, A. A.; Sundermeyer, J.; Schindler, S.; Karlin, K. D. Reactions of a Copper (II) Superoxo Complex Lead to C–H and O–H Substrate Oxygenation: Modeling Copper-Monooxygenase C–H Hydroxylation. *Angewandte Chemie International Edition* **2008,** *47*, 82-85.

6.   Maiti, D.; Fry, H. C.; Woertink, J. S.; Vance, M. A.; Solomon, E. I.; Karlin, K. D. A 1: 1 Copper−Dioxygen Adduct is an End-on Bound Superoxo Copper (II) Complex which Undergoes Oxygenation Reactions with Phenols. *Journal of the American Chemical Society* **2007,** *129*, 264-265.

7.   Neuba, A.; Rohrmüller, M.; Hölscher, R.; Schmidt, W. G.; Henkel, G. A panel of peralkylated sulfur–guanidine type bases: Novel pro-ligands for use in biomimetic coordination chemistry. *Inorganica Chimica Acta* **2015,** *430*, 225-238.

8.   Mader, E. A.; Davidson, E. R.; Mayer, J. M. Large Ground-State Entropy Changes for Hydrogen Atom Transfer Reactions of Iron Complexes. *Journal of the American Chemical Society* **2007,** *129*, 5153-5166.

9.   Wu, A.; Mader, E. A.; Datta, A.; Hrovat, D. A.; Borden, W. T.; Mayer, J. M. Nitroxyl Radical Plus Hydroxylamine Pseudo Self-Exchange Reactions: Tunneling in Hydrogen Atom Transfer. *Journal of the American Chemical Society* **2009,** *131*, 11985-11997.

10.   Fulmer, G. R.; Miller, A. J. M.; Sherden, N. H.; Gottlieb, H. E.; Nudelman, A.; Stoltz, B. M.; Bercaw, J. E.; Goldberg, K. I. NMR Chemical Shifts of Trace Impurities: Common Laboratory Solvents, Organics, and Gases in Deuterated Solvents Relevant to the Organometallic Chemist. *Organometallics* **2010,** *29*, 2176-2179.

11.   Tenderholt, A.; Hedman, B.; Hodgson, K. O. PySpline: A Modern, Cross-Platform Program for the Processing of Raw Averaged XAS Edge and EXAFS Data. *AIP Conference Proceedings* **2007,** *882*, 105-107.

12.   Rehr, J. J.; Albers, R. C. Theoretical approaches to x-ray absorption fine structure. *Reviews of Modern Physics* **2000,** *72*, 621-654.

13.   Neese, F. Software update: the ORCA program system, version 4.0. *WIREs Computational Molecular Science* **2018,** *8*, e1327.

14.   Neese, F.; Wennmohs, F.; Hansen, A.; Becker, U. Efficient, approximate and parallel Hartree-Fock and hybrid DFT calculations. A 'chain-of-spheres' algorithm for the Hartree-Fock exchange. *Chemical Physics* **2009,** *356*, 98.

15.   Becke, A. D. Density-functional exchange-energy approximation with correct asymptotic behavior. *Physical Review A* **1988,** *38*, 3098-3100.

16.   Lee, C.; Yang, W.; Parr, R. G. Development of the Colle-Salvetti correlation-energy formula into a functional of the electron density. *Physical Review B* **1988,** *37*, 785-789.

17.   Grimme, S.; Ehrlich, S.; Goerigk, L. Effect of the damping function in dispersion corrected density functional theory. *Journal of Computational Chemistry* **2011,** *32*, 1456-1465.

18.   Grimme, S.; Antony, J.; Ehrlich, S.; Krieg, H. A consistent and accurate ab initio parametrization of density functional dispersion correction (DFT-D) for the 94 elements H-Pu. *The Journal of Chemical Physics* **2010,** *132*, 154104.

19.   Weigend, F.; Ahlrichs, R. Balanced basis sets of split valence, triple zeta valence and quadruple zeta valence quality for H to Rn: Design and assessment of accuracy. *Physical Chemistry Chemical Physics* **2005,** *7*, 3297-3305.

20.   Weigend, F. Accurate Coulomb-fitting basis sets for H to Rn. *Physical Chemistry Chemical Physics* **2006,** *8*, 1057-1065.

21.   Barone, V.; Cossi, M. Quantum Calculation of Molecular Energies and Energy Gradients in Solution by a Conductor Solvent Model. *The Journal of Physical Chemistry A* **1998,** *102*, 1995-2001.

22.   Bhadra, M.; Lee, J. Y. C.; Cowley, R. E.; Kim, S.; Siegler, M. A.; Solomon, E. I.; Karlin, K. D. Intramolecular hydrogen bonding enhances stability and reactivity of mononuclear cupric superoxide complexes. *Journal of the American Chemical Society* **2018,** *140*, 9042-9045.